Journal of Hazardous Materials 217–218 (2012) 36–42

Contents lists available at SciVerse ScienceDirect

Journal of Hazardous Materials

journal homepage: www.elsevier.com/locate/jhazmat

Facile, template-free synthesis of silver nanodendrites with high catalytic activity for the reduction of *p*-nitrophenol

Wei Zhang [a], Fatang Tan [a,*], Wei Wang [a], Xiaolin Qiu [b], Xueliang Qiao [a], Jianguo Chen [a]

[a] State Key Laboratory of Plastic Forming Simulation and Die and Mold Technology, Huazhong University of Science and Technology, Wuhan, 430074 Hubei, People's Republic of China
[b] Nanomaterials Research Center, Nanchang Institute of Technology, Nanchang, 330013 Jiangxi, People's Republic of China

ARTICLE INFO

Article history:
Received 26 September 2011
Received in revised form
30 November 2011
Accepted 17 January 2012
Available online 8 March 2012

Keywords:
Silver nanodendrites
Galvanic replacement reduction
Catalysts
p-Nitrophenol

ABSTRACT

Here we report a facile, surfactant-free and template-free synthesis process of highly uniform dendritic silver nanostructures with high catalytic activity for the reduction of *p*-nitrophenol. By controlling the concentration of $AgNO_3$ aqueous solution and the reaction time, various shapes of silver nanodendrites (SNDs) could be obtained easily. The effects of different parameters such as concentrations of the reagents and reaction time on the morphology and structure of as-prepared tree-like nanostructures have also been investigated by X-ray diffraction (XRD), field-emission scanning electron microscopy (FESEM) and transmission electron microscopy (TEM). Also, the X-ray photoelectron spectroscopy (XPS) has been used to identify the oxidation state of SNDs. In addition, the catalytic activity of the as-prepared SNDs samples at 200 mM $AgNO_3$ aqueous solution was evaluated by a redox reaction of *p*-nitrophenol in the presence of an excess amount of $NaBH_4$. It was found that the highly symmetrical SNDs with roughly 60–120 nm in stem and branch diameter and 3–12 μm in length obtained after 120 s reaction time do have higher catalytic activity than other SNDs prepared at different reaction time, several times stronger catalytic activity in the sodium borohydride reduction of *p*-nitrophenol to p-aminophenol, compared to some other silver nanoparticles reported in literature. The crystallinity provided by X-ray diffraction (XRD) analysis indicates that the improvement of the crystallinity is also very crucial for SNDs' catalytic activities. The SNDs are very promising catalytic candidates for the reduction of *p*-nitrophenol because of easily simple preparation route and high catalytic activity.

1. Introduction

Nitroaromatics are widely used as synthetic intermediates in the manufacture of pharmaceuticals, dyes, plasticizers, pesticides, fungicides, and explosives. Among the mono-nitrophenols, *p*-nitrophenol (Nip) is probably the most important in terms of the quantities, Meanwhile, *p*-nitrophenol possesses good chemical, biological stability and difficult to be removed by natural degradation, which has been listed as "priority pollutant" by US Environmental Protection Agency (EPA). Therefore, the *p*-nitrophenol in the waste water of chemicals, petrochemicals, and pharmaceuticals industries should be treated effectively and reasonably before discharged into the environment.

Many processes have been reported for oxidative or reductive degradation of nitrophenol compounds, such as catalytic wet peroxide oxidation [1], microwave assisted catalytic oxidation [2] biodegradation [3], photocatalytic degradation [4], electro-fenton method [5], electrochemical treatment [6], catalytic reduction [7,8] and so on. Among above methods, nanocatalysts in the facile reduction process of pollutants like *p*-nitrophenol has gained much attention, due to the greater accessibility to surface atoms and low coordination number. Metallic nanoparticles have been reported as catalysts for reduction of *p*-nitrophenol in many papers [9–12]. Taking the cost and the complicated synthesis process for such catalysts into account, we still need to find appropriate nanostructures for obtaining better catalytic activity. Recently, noble metal nanostructures, whose properties markedly differ from that of the respective bulk metals [13], are of considerable interest because of their importance in a wide range of applications including catalysis, photography, optics, electronics, optoelectronics, sensors, and surface-enhanced Raman scattering (SERS) [14–18]. Especially, silver nanodendrites (SNDs) have attracted rising interest due to their high specific surface area along with numerous active sites and sharp edges, which would provide a strong catalytic activity for facile reduction of *p*-nitrophenols.

The diversity of the technological applications of silver dendrites drives the search for facile routes to produce silver dendrites in high yields. Recent research for synthesis of such materials involved either chemical or electrochemical approaches, such as ultrasonically assisted template synthesis [19], ultraviolet

* Corresponding author.
E-mail address: fatangtan@hust.edu.cn (F. Tan).

0304-3894/$ – see front matter © 2012 Elsevier B.V. All rights reserved.
doi:10.1016/j.jhazmat.2012.01.056

irradiation photoreduction [20], plating [21], γ-irradiation route [22], and pulsed sonoelectrochemical method [23], Huang et al. synthesized Ag dendrites with an apparatus similarly used for electrodeposition with some modifications [24]. These approaches are complicated for synthesis or need water soluble polymers as protecting reagents or templates.

In recent years, galvanic replacement reaction (GRR) has been extensively used as a basic and simple way to synthesize nanostrucutured materials in a number of different systems [25–27]. Concentrating specifically on the template- and surfactant-free synthesis of Ag nanodendrites, Fang et al. reported a GRR process to synthesize SNDs using zinc plate as a sacrificial template [28]. Wen et al. synthesized silver nanodendrites by a simple surfactant-free method using a suspension of zinc microparticles as a heterogeneous reducing agent [29]. However, there is still some inconvenience in this synthesis process. Because the standard reduction potential of zinc (−0.7628 V) is much lower than that of silver (0.7996 V), resulting in the relatively fast speed of GRR process, which is not conducive to precisely control the morphology of SNDs.

More recently, Xie et al. successfully synthesized silver dendrite crystals by using an aqueous solution of silver ion and a Cu foil, assisted by sulfate ion, and found that the growth rate of Ag dendrites is much accelerated for a solution of Ag^+ with SO_4^{2-}, but the concentration of the silver ion is only 5 mM [30].

Nonetheless, a well-controlled large scale production protocol for silver nanodendrites is still in great demand and thus we embarked on research involving silver nanodendrites synthesis with a particular emphasis on high silver ion concentration and easy procedure. Consequently, our work provides a methodology that can be potentially scaled up in directly synthesizing silver nanodendrites, in which only copper reacts with $AgNO_3$ aqueous solution at room temperature to produce highly branched nanodendrites in seconds to a few minutes. No additional solvents, reducing agents or capping agents are necessary, making this synthetic protocol particularly attractive for studies into the formation of highly branched silver nanodendrites, which showed to be a novel catalyst for the reduction of *p*-nitrophenol.

2. Experimental

2.1. Materials

Silver nitrate ($AgNO_3$, 99.9%), sodium borohydride ($NaBH_4$) and *p*-nitrophenol (4-$C_6H_5NO_3$) were purchased from Sinopharm Chemical Reagent Co., Ltd. (SCRC). Copper foil (99.9%) was obtained from Hubei Xinyin Noble Metal Co., Ltd. All reagents were of analytical grade and used without further purification. All solutions were prepared using double distilled water.

2.2. Synthesis of SNDs

In a typical synthesis of Ag dendrites, copper foils were cut into $2 \times 2\,cm^2$ and treated by dilute hydrochloric acid solution to remove oxide and contamination, then, rinsed with distilled water. After rinsing in water, the copper foils were immediately immersed in a 200 mM $AgNO_3$ aqueous solution. After some time, the copper foils were taken out the $AgNO_3$ aqueous solution and immediately immersed in distilled water; SNDs were detached from the copper foils by rinsing in water and then filtered and dried in air, by adjusting reaction time, different morphologies of silver nanostructures were obtained. Finally, as-prepared SNDs were redispersed in ethanol for further characterization. Similar sets of reactions were also carried out at varying $AgNO_3$ concentration; i.e., 100 mM and 300 mM.

2.3. Characterization and catalytic reduction of p-nitrophenol

The morphologies of the samples were investigated by FESEM (Sirion200, FEI Company, Holland) at 10 kV and TEM (Tecnai G220, FEI Company, Holland) at 120 kV. The oxidation state of SNDs was verified by X-ray photoelectron spectroscopy (XPS; VG Multilab 2000, Thermo Electron Corporation, US) with a microspot monochromatized Al K_α source, both survey and high-resolution spectra were acquired in fixed analyzer transmission mode with a pass energy of 100 and 25 eV, respectively. The phase structures were determined by using X-ray diffraction (XRD; X'Pert PRO (PANalytical B.V., Holland)) on a Scintag diffractometer with Cu $K_{\alpha1}$ radiation (λ = 1.54060 Å) at a scanning rate of $0.017^\circ\,s^{-1}$ in the 2θ range from 10° to 90°. BET surface area measurements were carried out in a gas adsorption analyzer (Tristar 3000, Micromeritics Company, US). In each experiment, a weight of approximately 0.1 g of sample was used. The adsorptive gas was nitrogen (N_2) and the adsorption was carried out at the boiling temperature of liquid nitrogen.

In a typical run for the reduction of *p*-nitrophenol by $NaBH_4$, 0.1 ml of freshly prepared aqueous solution of $NaBH_4$ (3×10^{-1} M) was introduced to 3 ml of *p*-nitrophenol (1.03×10^{-4} M) solution. Next, 2 mg of SNDs was added to the above solution, and time-dependent absorption spectra were recorded. From changes in the absorption of *p*-nitrophenolate ion at 400 nm as a function of time, the rate constants were calculated. The UV–vis absorption spectra were recorded in a Shimadzu UV-2550 spectrophotometer. The experiment was carried out at 20 °C.

3. Results and discussion

Galvanic replacement reaction has been demonstrated as a type of general and effective means for preparing metallic nanostructures by consuming the more reactive component [31]. Copper has a relatively higher standard reduction potential (0.3402 V) than zinc, which makes the GRR mild and easy to control. In addition, no copper oxides exist in the final product, which was verified by the result of X-ray diffraction analysis in our experiment. Since the standard reduction potential of Ag^+/Ag pair (0.7996 V vs SHE) is higher than that of the Cu^{2+}/Cu pair (0.34 V vs SHE), copper undergoes a GRR with Ag^+ ions when copper foil is immersed in $AgNO_3$ solution according to the following equation:

$$Cu(s) + 2Ag^+(aq) \rightarrow 2Ag(s) + Cu^{2+}(aq) \quad (1)$$

Fig. 1 shows a TEM image of SNDs prepared at 200 mM $AgNO_3$ aqueous solution after 120 s reaction time, where the insets are selected-area electron diffraction (SAED) patterns from the area indicated by red circle in Fig. 1. The large surface area suggests these dendrites as promising catalysts, as they also present a high concentration of edges and terraces, features that are believed to provide stronger signal for SERS [32]. Meanwhile, the SAED confirms that the crystallinity of the silver nanodendrite is perfect. As shown in this image, the electron beam is perpendicular to the flat surface of the nanodendrite lying on the TEM grid which displays regular lattices characteristic of the cubic Ag, it was proved that the silver nanodendrite is a single crystal. The electron beam also illustrates that the growth of SND is along two specific crystal planes alternately. By analyzing this term of beam, we found that SAED patterns are indexed as {2 2 0} and formally forbidden 1/3 {4 2 2} Bragg reflections, which is similar to the previous reports [33].

Furthermore, the surface elemental composition of the as-prepared SNDs at 200 mM $AgNO_3$ aqueous solution after 120 s reaction time was studied by means of XPS. A typical wide-scan spectrum is shown in Fig. 2(a), Ag signals, such as the Ag3d doublet, and a number of secondary photoemission and Ag Auger

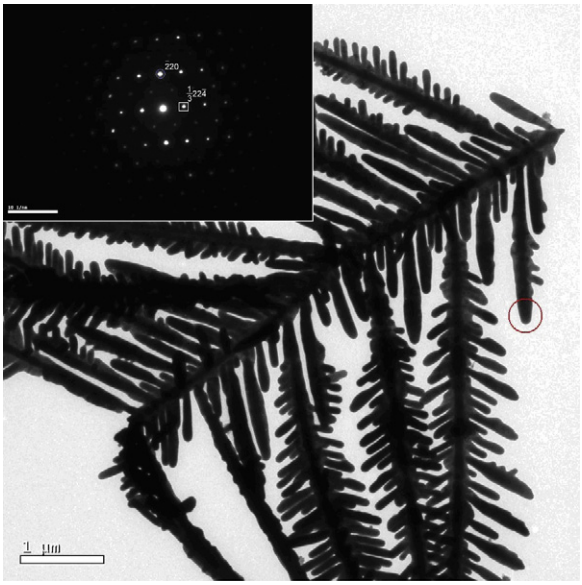

Fig. 1. TEM image with SAED pattern (inset) of a typical silver nanodendrite prepared at 200 mM $AgNO_3$ aqueous solution after 120 s reaction time. (For interpretation of the references to color in this text, the reader is referred to the web version of the article.)

peaks (Ag4d, Ag4p, Ag4s, Ag3p, Ag3s) are clearly seen in the wide-scan spectrum. Although the carbon and oxygen signals are also detected, they exhibit lower concentrations. Fig. 2(b) shows the high resolution XPS of Ag3d peaks with binding energies of 368.0 eV for Ag3d5/2 and 374.1 eV for Ag3d3/2, indicating that the SNDs are mainly elemental Ag [30].

3.1. Effects of $AgNO_3$ concentration on the morphology of SNDs

The $AgNO_3$ concentration has important influences on the size and morphology of the products during the replacement reaction, the higher Ag^+ concentration enhances the reaction rate greatly, thereby leading to changes in the morphology of SNDs. Figs. 3 and 4(a) demonstrate the transition from half baked to dendritic growth of silver aggregates at silver ion concentration of 100, 300 mM and 200 mM after 10 s reaction time under room temperature. As shown in Figs. 3 and 4(a), at the same reaction time, appropriate concentration would synthesize expected nanodendrites in a short time, while low concentration led to incomplete morphologies (Fig. 3(a)). On the contrary, higher concentration will not help the controllable formation of nanodendritic silver structures due to too fast reaction (Fig. 3(b)). This experiment indicates that, by controlling the silver ion concentration in the solution, a silver dendrite with well-defined morphology could be realized (Fig. 4(a)).

3.2. Morphological evolution and crystallinity of SNDs with time

To better understand how these SNDs form with time, we controlled the reaction time to explore the nano/microstructure evolution of silver. FESEM images of SNDs were obtained for different reaction time. Fig. 4 shows FESEM images of the dendrites synthesized at 200 mM $AgNO_3$ aqueous solution with different reaction time: 10 s, 60 s, and 120 s, which were denoted as Ag1, Ag2 and Ag3, respectively. As Fig. 4(a) reveals, the dendritic nanostructure had been synthesized during 10 s of reaction. Next, as the reaction proceeded to 60 s, additional precursor reduction occurred in which silver atoms were added to the bulbous ends of the branch, the two-terminal dendritic nanostructures become thicker and

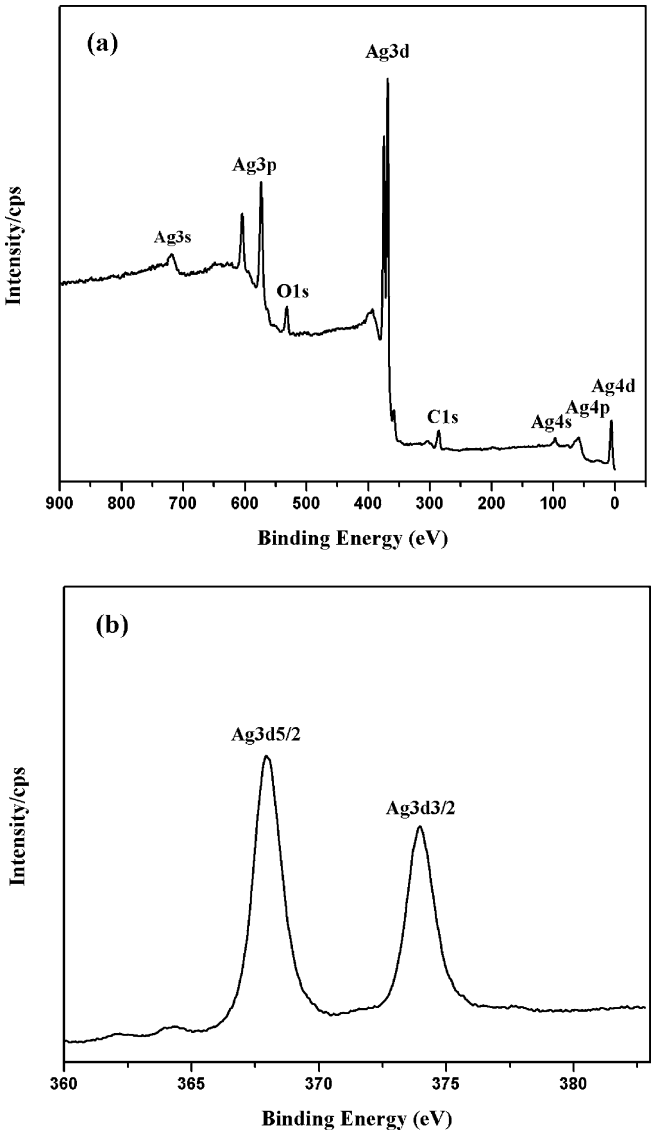

Fig. 2. Typical X-ray photoelectron spectroscopy wide-scan spectrum (a) and high resolution XPS Ag3d peaks of SNDs (b) prepared at 200 mM $AgNO_3$ aqueous solution after 120 s reaction time.

more complete, at the same time, a few Ag particles adhere to the branches to form the third class structures (Fig. 4(b)). After 120 s, mature SNDs with symmetrical tertiary structures like a pine tree with roughly 60–120 nm in stem and branch diameter and 3–12 μm in length were formed (Fig. 4(c)).

The diffusion-limited aggregation (DLA) model and the anisotropic crystal growth can also be used to interpret the evolution of SNDs [34]. In the case of dendritic nanostructures, the thermodynamic factors and the inherent crystal structure of the material are two major factors, which dominate the ensuing morphology during the GRR process. At the beginning of this reaction, the preferred growth on certain planes becomes energetically favorable when the surface tensions of these planes are elevated and the bulk energy of the total system tends to decline [35]. The result is that silver particles aggregate dendritic rather than a thermodynamically stable hexagonal structure. It is well established that fractal aggregation arises in situations far from thermodynamic equilibrium where high driving forces lead to the generation of dendrites and random self-assembly [36].

Fine crystallinity and big surface area usually result in pronounced catalytic activity. Fig. 5 shows XRD patterns of the three

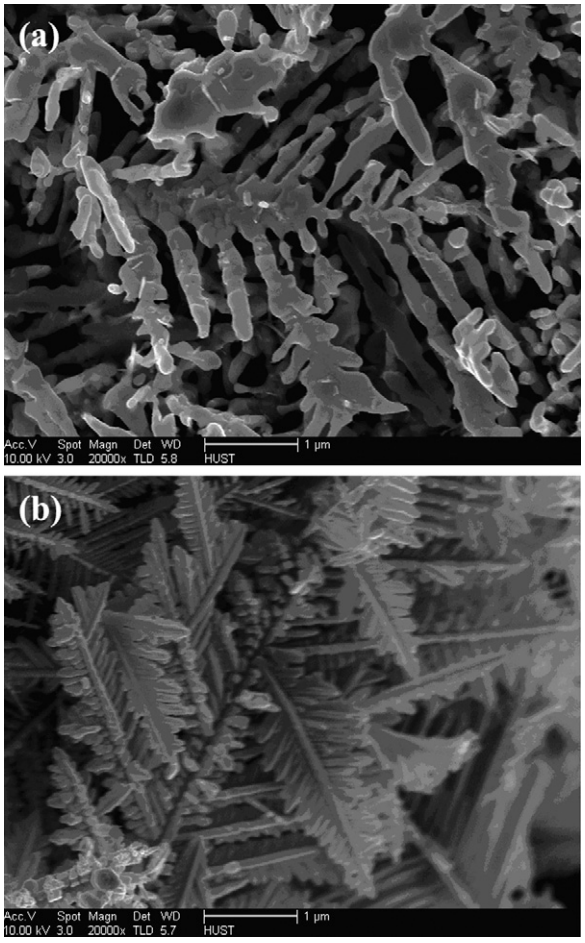

Fig. 3. FESEM images of as-prepared SNDs at different concentration of $AgNO_3$ aqueous solution for 10 s (a) 100 mM, (b) 300 mM.

samples Ag1, Ag2 and Ag3. All the diffraction peaks observed can be indexed to the cubic (FCC) Ag with a unit cell parameter $a = b = c = 4.0816$ Å (4.0862 Å, from JCPDS 04-0783). No copper or copper oxide peak is observed, indicating a useful method to synthesize high-purity Ag nanodendrites. Furthermore, the crystallinity is different for the three samples. The order of the crystallinity of the three SNDs is: Ag3 > Ag2 > Ag1.

3.3. Catalytic activities of SNDs in the sodium borohydride reduction of p-nitrophenol

One of the important applications of metal nanoparticles is to activate/catalyze some reactions that are otherwise unfeasible. It is well-known that the catalytic activity of nanoparticles is strongly dependent on its composition, size, and shape. Typically, a bigger surface-to-volume ratio tends to show a higher catalytic activity [37,38]. To this end, the reduction of *p*-nitrophenol (Nip) to p-aminophenol (Amp) by $NaBH_4$ was chosen to evaluate the catalytic activity of SNDs (Ag1, Ag2 and Ag3, respectively). The reaction was monitored visually as well as spectrophotometrically by measuring the disappearance of Nip, which shows a distinct spectral profile with an absorption maximum at 317 nm in water, upon the addition of $NaBH_4$, the mixture solution shows a bright yellow color and with a shift to 400 nm due to the formation of the *p*-nitrophenolate ion [39,40], it also shows that no conversion from *p*-nitrophenol to *p*-aminophenol was observed without the addition of SNDs catalyst. This observation indicates that the reduction reaction was unable to occur by itself under the experimental conditions without the addition of catalysts.

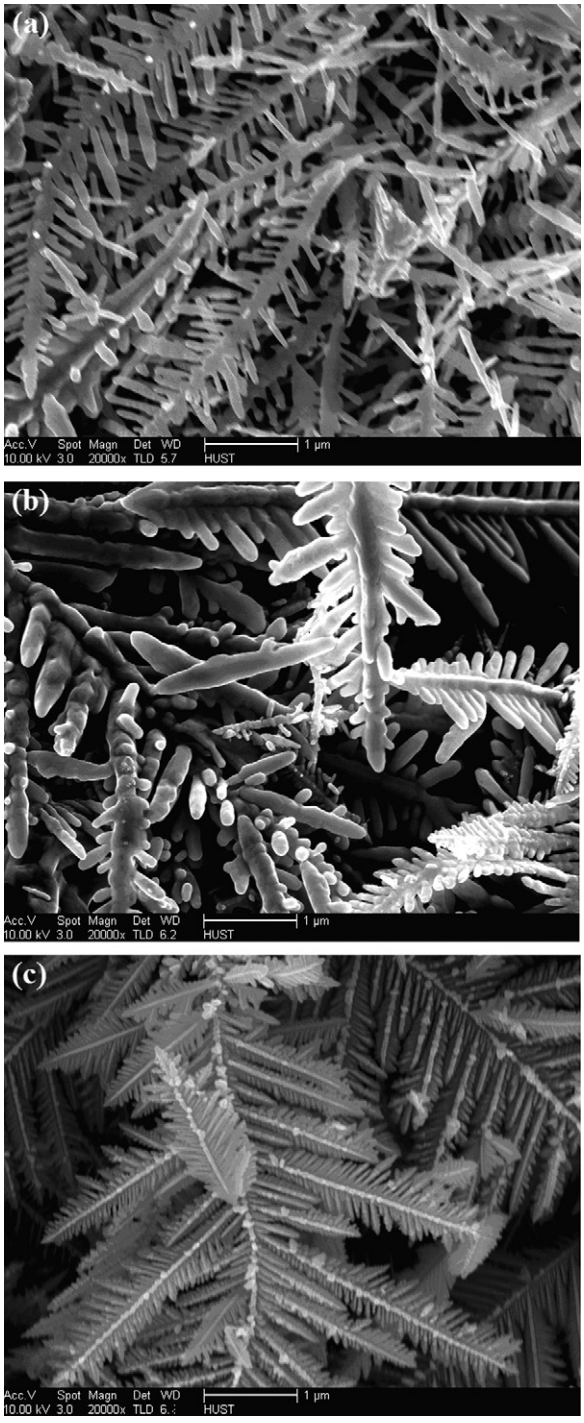

Fig. 4. FESEM images of as-prepared SNDs in the 200 mM $AgNO_3$ aqueous solution for reaction time of (a) 10 s (Ag1), (b) 60 s (Ag2), and (c) 120 s (Ag3).

However, after the addition of a small amount of SNDs (Ag1) to this solution at room temperature (20 °C), the color of the mixture solution is fading and ultimate bleaching in quick succession, the peak at 400 nm gradually drops in intensity which accompanied by a concomitant development of a new peak at 295 nm corresponding to the formation of *p*-aminophenol (Fig. 6(a)). Similar spectral changes of *p*-nitrophenol during its reduction are also observed with addition of other two samples Ag2 and Ag3 (Fig. 6(b) and (c)). These results indicate that SNDs are an effective catalyst in this reaction.

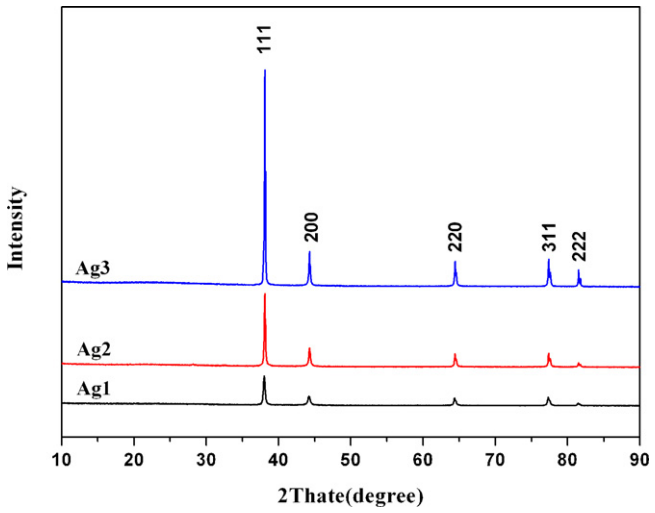

Fig. 5. XRD patterns of Ag nanodendrites synthesized with different reaction time.

As shown in Fig. 6, Ag3 shows the shortest time for *p*-nitrophenol to convert to *p*-aminophenol completely, in comparison with other two samples Ag1 and Ag2. The order of the catalytic activity for the three samples is Ag3 > Ag2 > Ag1. This trend is in accordance with the crystallinity of the samples.

Since the concentration of $NaBH_4$ greatly exceeded that of *p*-nitrophenol and the SNDs catalysts, the rates of the reduction are assumed to be only dependent of the concentration of *p*-nitrophenol (c_{Nip}). Therefore, the rate is assumed to follow first order kinetics [12]. Hence, the apparent rate constant (k_{app}) can be defined through

$$\frac{dc_{Nip}}{dt} = -k_{app}c_{Nip} \quad (2)$$

As the result, it allows us to use K_{app} to compare the catalytic activity of different kinds of nanoparticles. We calculated the values of K_{app} of SNDs defined through Eq. (2), which is obtained from the fit linear of lnA (A = absorbance at 400 nm of *p*-nitrophenolate ion, Fig. 6(a–c)) vs time (Fig. 6(d)). Because of the induction time at the beginning (will be discussed in the following part), all the data of Fig. 6(d) are selected from the second peak of absorbance at 400 nm in each UV–vis spectroscopy. The K_{app} of Ag3 is $5.63 \times 10^{-3}\ s^{-1}$ which is ten times bigger than that of silver nanoparticles reported in a recent paper, whose K_{app} is $4.73 \times 10^{-4}\ s^{-1}$ [41]. Furthermore,

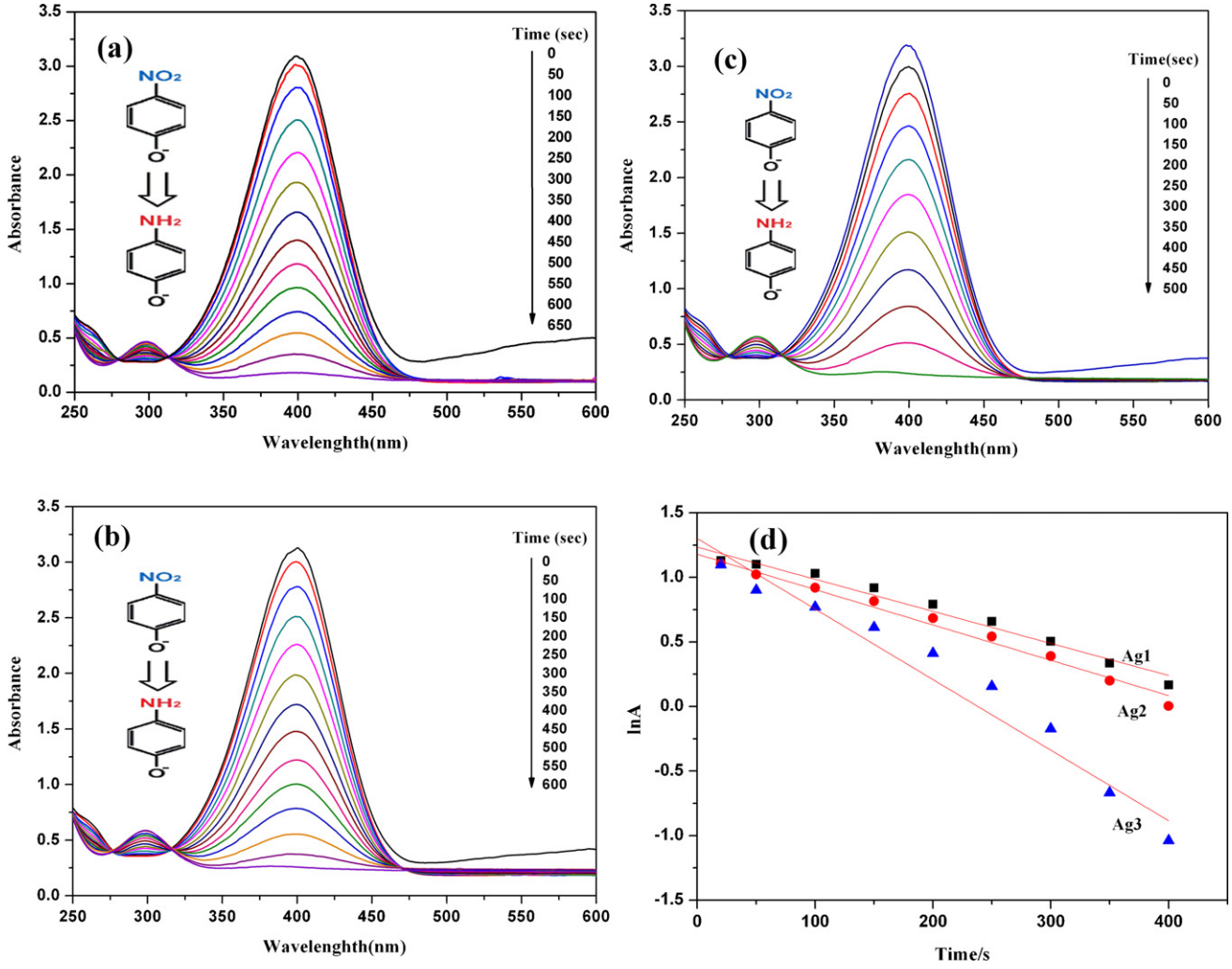

Fig. 6. (a–c) Successive UV–vis absorption spectra of *p*-nitrophenol reduction by $NaBH_4$ catalyzed by different samples of SNDs: (a) Ag1, (b) Ag2, (c) Ag3 at room temperature (20 °C). In all the cases, the quantity of the SNDs was 0.0185 mmol. (d) Plots of lnA vs time for the Ag1, Ag2, and Ag3 catalytic reduction of *p*-nitrophenol at room temperatures (20 °C).

Table 1
Summary of the catalytic activity for the reduction of *p*-nitrophenol by $NaBH_4$ which was catalyzed by different SNDs at room temperatures (20 °C).

Sample ID	SNDs used (mmol)	K_{app} (s^{-1})	K_{nor} ($mmol^{-1}\ s^{-1}$)
Ag1	0.0185	2.48×10^{-3}	0.134
Ag2	0.0185	2.74×10^{-3}	0.148
Ag3	0.0185	5.63×10^{-3}	0.304

to compare the catalytic activity of the as-prepared SNDs with that of other nanoparticles reported in the literatures [42–44], we calculated the normalized rate constant (K_{nor}) which are obtained by normalizing the K_{app} values with respect to the amount of catalysts used (summarized in Table 1). As shown in Table 1, we can find that the K_{nor} of Ag3 is 0.304 $mmol^{-1}\ s^{-1}$ (20 °C), which is larger than that of many catalysts reported previously [42,45,46], 0.069, 0.140 and 0.00037 $mmol^{-1}\ s^{-1}$ respectively. And the K_{app} of sample Ag3 is just a little smaller than that of an Au–Ag bimetallic dendritic nanostructure [24]. This is especially striking when the facile template-free synthesis and relatively cheap price of silver are taken into account. Combined with the amount of catalysts used in this reduction is a little; we can predict a wide application of SNDs in catalytic fields in the future.

Usually, the catalytic activity is positively related with the surface area of catalysts. However, in this work, higher surface areas of the catalysts did not result in higher catalytic performance. The BET surface areas of the as-prepared Ag1, Ag2 and Ag3 are 1.2602, 0.3901 and 0.3895 m^2/g, respectively. There was no correlation between the BET surface areas and the catalytic activities, demonstrating there is another more important factor that governs the catalytic activity, which is the crystallinity of the SNDs. The order of the crystallinity of the three SNDs is: Ag3 > Ag2 > Ag1.The result indicates that there is a compromise between the improvement of the crystallinity and the decrease of the surface area.

Another interesting observation is that there is an induction period for all the reactions after the adding of SNDs, due to the adsorption of *p*-nitrophenol on the surface of SNDs [47]. As can be seen from Fig. 6(a–c), the dropping value of the spectral peak at 400 nm during the first 50 s is smaller than that of successive time period, after this special stage, the speed of the value dropping at 400 nm is almost the constant, and the Ag3 still shows the shortest induction time compared to other samples. Because of the best catalytic activity of Ag3, we investigate the interaction of *p*-nitrophenol with the SNDs directly to see if Ag3 also perform better than other two SNDs. The UV–vis absorption spectra of *p*-nitrophenol solution were recorded after the addition of three types of SNDs respectively in absence of the reducing agent $NaBH_4$. As shown in Fig. 7, after the addition of SNDs, the characteristic absorption peak at 317 nm exhibits different levels of decrease. At the same time, a shoulder peak arises around 400 nm, which was related to the absorption spectra of intermediate of *p*-nitrophenol with SNDs. Among the three catalysts, Ag3 shows the most efficient effort for the absorption peak drops at 317 nm with a strongest shoulder peak around 400 nm. Ag2 shows a little stronger effort than Ag1. Though many papers have explained the mechanism of this catalytic reaction through models of Laugmuir–Hinshelwood or Eley-Rideal mechanism [48], the accurate reaction mechanism has not been distinguished. This result may be provided a hint for the further study.

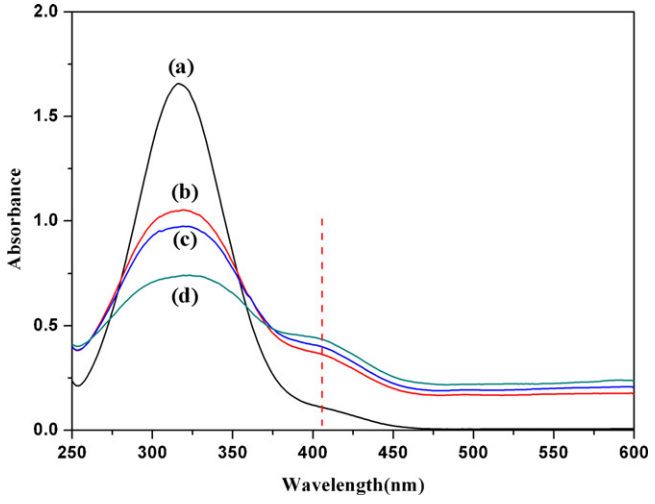

Fig. 7. UV–vis spectra of *p*-nitrophenol solution. (a) In absence of $NaBH_4$ and SNDs, (b–d) absence of $NaBH_4$ but adding 0.0185 mmol of three different types of SNDs, respectively: (b) Ag1, (c) Ag2, (d) Ag3.

4. Conclusions

In conclusion, a facile and efficient method has been successfully developed for the synthesis of silver nanodendrites by a galvanic replacement reaction (GRR) technique using copper foil as a sacrificial template. The catalytic activities of the hierarchical dendritic microstructures prepared under different conditions have been investigated carefully for the reduction of *p*-nitrophenol by $NaBH_4$. We have also demonstrated that mature and higher crystallinity of dendritic nanostructure shows better catalytic activity than immature samples. Given the facile synthesis, high catalytic activity and relatively low cost, the SNDs might be able to find wide application for the catalytic reduction of nitrophenol compounds.

Acknowledgements

Some ideas are inspired from the postdoctoral work supported by China Council-Georgetown University Scholarship Post-Doctoral Fellowship Program and Professor Tong's group in Georgetown University. The authors are grateful for the financial support provided by the National Basic Research Program of China (2009CB939705), National Natural Science Foundation of China (50902054), the Fundamental Research Funds for the Central Universities (C2009Q011) and Science Foundation of Hubei Province (2010CDB00501); we would also like to thank Analytical and Testing Center, Huazhong University of Science and Technology, P.R. China, for the TEM, FESEM and XRD test.

References

[1] R.M. Liou, S.H. Chen, C.H. Huang, C.L. Lai, C.Y. Shih, J.S. Chang, M.Y. Hung, Catalytic wet peroxide oxidation of *p*-nitrophenol by Fe (III) supported on resin, Water Sci. Technol. 62 (2010) 1879–1887.
[2] L.L. Bo, Y.B. Zhang, X. Quan, B. Zhao, Microwave assisted catalytic oxidation of *p*-nitrophenol in aqueous solution using carbon-supported copper catalyst, J. Hazard. Mater. 153 (2008) 1201–1206.
[3] V.L. Gemini, A. Gallego, V.M. de Oliveira, C.E. Gomez, G.P. Manfio, S.E. Korol, Biodegradation and detoxification of *p*-nitrophenol by *Rhodococcus wratislaviensis*, Int. Biodeteriorat. Biodegradat. 55 (2005) 103–108.
[4] C.L. Torres-Martinez, R. Kho, O.I. Mian, R.K. Mehra, Efficient photocatalytic degradation of environmental pollutants with mass-produced ZnS nanocrystals, J. Colloid Interface Sci. 240 (2001) 525–532.
[5] M.A. Oturan, J. Peiroten, P. Chartrin, A.J. Acher, Complete destruction of *p*-nitrophenol in aqueous medium by electro-Fenton method, Environ. Sci. Technol. 34 (2000) 3474–3479.
[6] C. Borras, T. Laredo, B.R. Scharifker, Competitive electrochemical oxidation of *p*-chlorophenol and *p*-nitrophenol on Bi-doped PbO(2), Electrochim. Acta 48 (2003) 2775–2780.
[7] Y.-C. Chang, D.-H. Chen, Catalytic reduction of 4-nitrophenol by magnetically recoverable Au nanocatalyst, J. Hazard. Mater. 165 (2009) 664–669.
[8] T. Swathi, G. Buvaneswari, Application of $NiCo_2O_4$ as a catalyst in the conversion of *p*-nitrophenol to *p*-aminophenol, Mater. Lett. 62 (2008) 3900–3902.
[9] N. Pradhan, A. Pal, T. Pal, Catalytic reduction of aromatic nitro compounds by coinage metal nanoparticles, Langmuir 17 (2001) 1800–1802.

[10] R. Narayanan, M.A. El-Sayed, Changing catalytic activity during colloidal platinum nanocatalysis due to shape changes: electron-transfer reaction, J. Am. Chem. Soc. 126 (2004) 7194–7195.
[11] Y. Mei, Y. Lu, F. Polzer, M. Ballauff, M. Drechsler, Catalytic activity of palladium nanoparticles encapsulated in spherical polyelectrolyte brushes and core-shell microgels, Chem. Mater. 19 (2007) 1062–1069.
[12] M.H. Rashid, T.K. Mandal, Templateless synthesis of polygonal gold nanoparticles: an unsupported and reusable catalyst with superior activity, Adv. Funct. Mater. 18 (2008) 2261–2271.
[13] C. Burda, X. Chen, R. Narayanan, M.A. El-Sayed, Chemistry and properties of nanocrystals of different shapes, Chem. Rev. (Washington, DC, US) 105 (2005) 1025–1102.
[14] W.P. Halperin, Quantum size effects in metal particles, Rev. Mod. Phys. 58 (1986) 533–606.
[15] J.P. Novak, L.C. Brousseau, F.W. Vance, R.C. Johnson, B.I. Lemon, J.T. Hupp, D.L. Feldheim, Nonlinear optical properties of molecularly bridged gold nanoparticle arrays, J. Am. Chem. Soc. 122 (2000) 12029–12030.
[16] S. Chen, Y. Yang, Magnetoelectrochemistry of gold nanoparticle quantized capacitance charging, J. Am. Chem. Soc. 124 (2002) 5280–5281.
[17] A.G. Tkachenko, H. Xie, D. Coleman, W. Glomm, J. Ryan, M.F. Anderson, S. Franzen, D.L. Feldheim, Multifunctional gold nanoparticle–peptide complexes for nuclear targeting, J. Am. Chem. Soc. 125 (2003) 4700–4701.
[18] P.M. Tessier, O.D. Velev, A.T. Kalambur, J.F. Rabolt, A.M. Lenhoff, E.W. Kaler, Assembly of gold nanostructured films templated by colloidal crystals and use in surface-enhanced raman spectroscopy, J. Am. Chem. Soc. 122 (2000) 9554–9555.
[19] J.P. Xiao, Y. Xie, R. Tang, M. Chen, X.B. Tian, Novel ultrasonically assisted templated synthesis of palladium and silver dendritic nanostructures, Adv. Mater. 13 (2001) 1887–1891.
[20] Y. Zhou, S.H. Yu, C.Y. Wang, X.G. Li, Y.R. Zhu, Z.Y. Chen, A novel ultraviolet irradiation photoreduction technique for the preparation of single-crystal Ag nanorods and Ag dendrites, Adv. Mater. 11 (1999) 850–852.
[21] V. Fleury, W.A. Watters, L. Allam, T. Devers, Rapid electroplating of insulators, Nature 416 (2002) 716–719.
[22] S. Wang, H. Xin, Fractal and dendritic growth of metallic Ag aggregated from different kinds of γ-irradiated solutions, J. Phys. Chem. B 104 (2000) 5681–5685.
[23] Y. Socol, O. Abramson, A. Gedanken, Y. Meshorer, L. Berenstein, A. Zaban, Suspensive electrode formation in pulsed sonoelectrochemical synthesis of silver nanoparticles, Langmuir 18 (2002) 4736–4740.
[24] J. Huang, S. Vongehr, S. Tang, H. Lu, J. Shen, X. Meng, Ag dendrite-based Au/Ag bimetallic nanostructures with strongly enhanced catalytic activity, Langmuir 25 (2009) 11890–11896.
[25] H. Lin, J. Mock, D. Smith, T. Gao, M.J. Sailor, Surface-enhanced raman scattering from silver-plated porous silicon, J. Phys. Chem. B 108 (2004) 11654–11659.
[26] Y. Sun, Y. Xia, Mechanistic study on the replacement reaction between silver nanostructures and chloroauric acid in aqueous medium, J. Am. Chem. Soc. 126 (2004) 3892–3901.
[27] G.S. Metraux, Y.C. Cao, R. Jin, C.A. Mirkin, Triangular nanoframes made of gold and silver, Nano Lett. 3 (2003) 519–522.
[28] J. Fang, H. You, P. Kong, Y. Yi, X. Song, B. Ding, Dendritic silver nanostructure growth and evolution in replacement reaction, Cryst. Growth Des. 7 (2007) 864–867.
[29] X.G. Wen, Y.T. Xie, W.C. Mak, K.Y. Cheung, X.Y. Li, R. Renneberg, S. Yang, Dendritic nanostructures of silver: facile synthesis, structural characterizations, and sensing applications, Langmuir 22 (2006) 4836–4842.
[30] S. Xie, X. Zhang, D. Xiao, M.C. Paau, J. Huang, M.M.F. Choi, Fast growth synthesis of silver dendrite crystals assisted by sulfate ion and its application for surface-enhanced raman scattering, J. Phys. Chem. C 115 (2011) 9943–9951.
[31] L.A. Porter, H.C. Choi, A.E. Ribbe, J.M. Buriak, Controlled electroless deposition of noble metal nanoparticle films on germanium surfaces, Nano Lett. 2 (2002) 1067–1071.
[32] A. Gutés, C. Carraro, R. Maboudian, Silver dendrites from galvanic displacement on commercial aluminum foil as an effective SERS substrate, J. Am. Chem. Soc. 132 (2010) 1476–1477.
[33] V. Germain, J. Li, D. Ingert, Z.L. Wang, M.P. Pileni, Stacking faults in formation of silver nanodisks, J. Phys. Chem. B 107 (2003) 8717–8720.
[34] R.M. Brady, R.C. Ball, Fractal growth of copper electrodeposits, Nature 309 (1984) 225–229.
[35] K.-Q. Zhang, X.Y. Liu, In situ observation of colloidal monolayer nucleation driven by an alternating electric field, Nature 429 (2004) 739–743.
[36] M. Wang, X.-Y. Liu, C.S. Strom, P. Bennema, W. van Enckevort, N.-B. Ming, Fractal and aggregations at low driving force with strong anisotropy, Phys. Rev. Lett. 80 (1998) 3089–3092.
[37] M.-C. Daniel, D. Astruc, Gold nanoparticles: assembly supramolecular chemistry quantum-size-related properties, and applications toward biology, catalysis, and nanotechnology, Chem. Rev. (Washington, DC, US) 104 (2003) 293–346.
[38] B.K. Min, C.M. Friend, Heterogeneous gold-based catalysis for green chemistry: low-temperature CO oxidation and propene oxidation, Chem. Rev. (Washington, DC, US) 107 (2007) 2709–2724.
[39] K. Hayakawa, T. Yoshimura, K. Esumi, Preparation of gold – dendrimer nanocomposites by laser irradiation and their catalytic reduction of 4-nitrophenol, Langmuir 19 (2003) 5517–5521.
[40] S. Praharaj, S. Nath, S.K. Ghosh, S. Kundu, T. Pal, Immobilization recovery of Au nanoparticles from anion exchange resin: resin-bound nanoparticle matrix as a catalyst for the reduction of 4-nitrophenol, Langmuir 20 (2004) 9889–9892.
[41] X. Huang, Y. Xiao, W. Zhang, M. Lang, In-situ formation of silver nanoparticles stabilized by amphiphilic star-shaped copolymer and their catalytic application, Appl. Surf. Sci. 258 (2012) 2655–2660.
[42] M.H. Rashid, R.R. Bhattacharjee, A. Kotal, T.K. Mandal, Synthesis of spongy gold nanocrystals with pronounced catalytic activities, Langmuir 22 (2006) 7141–7143.
[43] D.M. Dotzauer, J. Dai, L. Sun, M.L. Bruening, Catalytic membranes prepared using layer-by-layer adsorption of polyelectrolyte/metal nanoparticle films in porous supports, Nano Lett. 6 (2006) 2268–2272.
[44] Y. Khalavka, J. Becker, C. Snnichsen, Synthesis of rod-shaped gold nanorattles with improved plasmon sensitivity and catalytic activity, J. Am. Chem. Soc. 131 (2009) 1871–1875.
[45] M.H. Rashid, T.K. Mandal, Synthesis and catalytic application of nanostructured silver dendrites, J. Phys. Chem. C 111 (2007) 16750–16760.
[46] K. Esumi, R. Isono, T. Yoshimura, Preparation of PAMAM- and PPI-metal (silver, platinum, and palladium) nanocomposites and their catalytic activities for reduction of 4-nitrophenol, Langmuir 20 (2003) 237–243.
[47] J. Zeng, Q. Zhang, J. Chen, Y. Xia, A comparison study of the catalytic properties of Au-based nanocages, nanoboxes, and nanoparticles, Nano Lett. 10 (2009) 30–35.
[48] H. Zhang, X. Li, G. Chen, Ionic liquid-facilitated synthesis and catalytic activity of highly dispersed Ag nanoclusters supported on TiO_2, J. Mater. Chem. 19 (2009) 8223–8231.